Delft University of Technology

Document Version
Final published version

Licence
CC BY

Citation (APA)
Fockaert, L. I., Pletincx, S., Boelen, B., Hauffman, T., Terryn, H., & Mol, J. M. C. (2020). Effect of zirconium-based conversion treatments of zinc, aluminium and magnesium on the chemisorption of ester-functionalized molecules. *Applied Surface Science*, *508*, Article 145199. https://doi.org/10.1016/j.apsusc.2019.145199

Important note
To cite this publication, please use the final published version (if applicable).
Please check the document version above.

Copyright
In case the licence states “Dutch Copyright Act (Article 25fa)”, this publication was made available Green Open Access via the TU Delft Institutional Repository pursuant to Dutch Copyright Act (Article 25fa, the Taverne amendment). This provision does not affect copyright ownership.
Unless copyright is transferred by contract or statute, it remains with the copyright holder.

Sharing and reuse
Other than for strictly personal use, it is not permitted to download, forward or distribute the text or part of it, without the consent of the author(s) and/or copyright holder(s), unless the work is under an open content license such as Creative Commons.

Takedown policy
Please contact us and provide details if you believe this document breaches copyrights.
We will remove access to the work immediately and investigate your claim.

This work is downloaded from Delft University of Technology.

Applied Surface Science 508 (2020) 145199

Contents lists available at ScienceDirect

Applied Surface Science

journal homepage: www.elsevier.com/locate/apsusc

Full Length Article

Effect of zirconium-based conversion treatments of zinc, aluminium and magnesium on the chemisorption of ester-functionalized molecules

L.I. Fockaert[a,b,c], S. Pletincx[d], B. Boelen[e], T. Hauffman[d], H. Terryn[d], J.M.C. Mol[c,*]

[a] Netherlands Organization for Scientific Research (NWO), Postbus 3021, 3502 GA Utrecht, the Netherlands
[b] Materials innovation institute (M2i), Elektronicaweg 25, 2628 XG Delft, the Netherlands
[c] Delft University of Technology, Department of Materials Science and Engineering, Research Group Corrosion Technology and Electrochemistry, Mekelweg 2, 2628 CD Delft, the Netherlands
[d] Vrije Universiteit Brussel, Department of Materials and Chemistry, Research Group Electrochemical Surface Engineering, Pleinlaan 2, 1050 Brussels, Belgium
[e] Tata Steel Ijmuiden B.V., Research and Development, Surface Engineering – Coating Development, 1970 CA Ijmuiden, the Netherlands

ARTICLE INFO

Keywords:
Zr-based conversion
Metal-molecule interaction
ATR-FTIR Kretschmann
XPS
Esters

ABSTRACT

The effect of zirconium-based conversion of thermally vaporized zinc, aluminium and magnesium on the chemisorption of dimethylsuccinate was studied using attenuated total reflection – Fourier transform infrared spectroscopy (ATR-FTIR) and X-ray photoelectron spectroscopy (XPS) analysis. Two competing chemisorption mechanisms contribute to interfacial bond formation. Hydrogen interactions on one hand were shown to occur between metal hydroxides and non-hydrolysed ester-groups of the molecule. On the other hand, both native and zirconium-treated substrates were shown to form interfacial carboxylate bonds with dimethylsuccinate, evidencing their capability of hydrolysing ester groups towards more reactive acid groups. Both interactions were shown to correlate to the metal oxide acid-base properties.

1. Introduction

Coil coated galvanized steel is frequently used in outdoor applications, mainly in the building sector for roof and cladding purposes. For durable use a high resistance against dry, wet and corrosive paint delamination is desired. Limited zinc resources, as well as more strict corrosion performance requirements, create a major industrial interest in shifting from conventional hot dipped galvanized steels to more corrosion resistant zinc-aluminium-magnesium based metallic coatings [1–3]. The addition of small amounts of magnesium results in two to four times longer corrosion protection than the standard zinc alloy [2,4]. Therefore, thinner, weight-saving coatings with comparable or even better performances are achieved while optimizing process costs. A disadvantage of zinc-magnesium alloys is the deteriorated adhesion to the underlying steel substrates [5]. This can be solved by adding aluminium to the alloy, at least equaling the level of magnesium, which at the same time offers the possibility of further improvements in corrosion protection. Although small amounts of aluminium and magnesium, typically below 2 wt%, are added to the zinc coating, due to migration effects, they are largely present at the surface where they form eutectic structures, consisting of zinc- and aluminium rich phases, and zinc-magnesium binary phases [1]. Both types of galvanized steel, being traditional hot dipped galvanized steel and zinc-aluminium-magnesium coated steel, undergo the same coil coat process steps and are thus being exposed to similar chemical treatments and paint finishes. Despite variations in surface composition, effective conversion and paint adhesion on both surfaces is required. Currently, zirconium- and titanium based conversion coatings are being used to replace, traditional conversion techniques such as hexavalent chromating and phosphating, which are subject to strict international health and safety regulations. These new generation of surface treatments are recognized as viable alternatives as they improve both corrosion resistance [6–12] and polymer adhesion [13–16]. Nevertheless, reported performances of zirconium-treated substrates are not always consistent, most likely because of the high variety in reported process parameters such as conversion time, precursor concentrations [11], organic [10] and inorganic [7,9] additives. Some authors attribute improved corrosion resistance to the formation of a more compact oxide layer, providing barrier properties [10,12]. Others highlight the elimination of surface potential differences at alloyed surfaces as major reason for enhanced corrosion resistance [11,17–19]. Investigations on paint adhesion are mainly based on macroscopic tests, such as pull off tests and roughness wettability measurements [13,15,19,20]. In this way, enhanced polymer adhesion has been ascribed to increased surface roughness [7,13] and

* Corresponding author.
E-mail address: J.M.C.Mol@tudelft.nl (J.M.C. Mol).

https://doi.org/10.1016/j.apsusc.2019.145199
Received 18 July 2019; Received in revised form 25 November 2019; Accepted 25 December 2019
Available online 28 December 2019
0169-4332/ © 2019 The Authors. Published by Elsevier B.V. This is an open access article under the CC BY license (http://creativecommons.org/licenses/by/4.0/).

increased wettability [15,21]. More fundamental chemisorption studies have been performed by Taheri et al. [16], who investigated the role of acid-base properties of converted zinc layers on the interfacial bond formation with succinc acid molecules. Since polyester resins are widely applied in coil coating and automotive paint, there is an industrial need to understand the effect of zirconium-based treatments on the adhesion of polyester primers. However, difficulties in studying chemisorption at paint-metal interfaces on a molecular level relate to the high absorptive character of both paint and metal substrate resulting in a buried interface. Moreover, complex multicomponent paint formulations hinder a straightforward interpretation of interfacial chemisorption mechanisms of the industrial paint/engineering metal system. Therefore, to gain fundamental insights in metal-polymer interactions, it is crucial to simplify the polymer chemistry [22]. One way to elucidate the molecular interactions at the polymer-metal interface is by mimicking the functional groups in polymer coatings using monomer molecules [23–25]. This approach offers the most freedom in selecting the organic chemistry of interest, which in case of industrially relevant polyester resins, are ester-functionalized compounds. Another way to model industrially-relevant polyester coatings is the thin film approach, where nanolayers of polymer films are applied by solvent evaporation. Both approaches allow the use of surface sensitive techniques, such as X-ray photoelectron spectroscopy (XPS), time-of-flight secondary ion mass spectroscopy (ToF-SIMS) and infrared reflection adsorption spectroscopy (IRRAS) to study interfacial interactions. The ease of modelling organic functionalities using simplified compounds has shown to result in important fundamental insights in interfacial interactions [26–33]. Contradictory IRRAS results on the capability of metal oxides to hydrolyse esters into carboxylic acids indicate the key-role of oxide acid-properties in the establishment of interfacial bonds [26–28]. Leadley and Watts [29] studied PMMA-metal interfaces performing XPS analysis. They reported that acidic metals such as silicon interact with PMMA through hydrogen bonds. Contrary, amphoteric substrates such as oxidized iron and aluminium were shown to be able to hydrolyse the methyl ester to form interfacial carboxylate bonds [29]. Konstadinidis et al. [30] and Papirer et al. [31] evaluated chemisorption of PMMA on aluminium using solid state NMR. A significant loss of methoxy carbon illustrated in the NMR spectra after adsorption supported the hypothesis of bond cleavage as a result of ester hydrolysis [30]. Tannenbaum et al. [32], reported the importance of water as a mediating agent in the chemisorption of PMMA to aluminium oxide. Hydrolysing the ester group forming carboxylic acids was believed not to be sufficient to establish chemical bonding at the aluminium oxide surface. A subsequent intermediate step, being the dissociation of acid to carboxylate anions in the presence of water, was considered as a requirement for chemisorption to occur [32]. Pletincx et al. [33] supported this statement using near-ambient XPS, ToF-SIMS and ATR-FTIR in Kretschmann geometry. More water at the interface was shown to lead to more ionic bond formation. At this point, the decisive role of metal oxide acid-base properties on the final chemisorption mechanism is evident. However, previous mechanistic studies are mostly limited to aluminium oxides, whereas the chemisorption of carboxylic acid compounds on industrially relevant zinc [34] and magnesium [35] are rather limited. Furthermore, in real-life applications, polymer coatings are rarely applied on native oxides. Moreover, it is well known that zirconium-based conversion of metal oxides is highly substrate dependent [16,36,37]. It is thus important to understand the effect of chemical pretreatments on the chemisorption of organic compounds.

This work presents a comparative study of the chemisorption of ester-functionalized monomers on aluminium, zinc and magnesium oxide. These metals were chosen because of their presence in industrially relevant zinc-aluminium-magnesium coatings used for galvanized steel. Variations in both galvanizing as well as coil coating process result in different surface compositions. To be able to relate the effect of metal oxide properties on the chemical interaction with organic compounds we have opted to study pure metal substrates. A comparative study is conducted on both native metal oxides as well as hexafluorozirconic acid- treated metal oxides. The use of hexafluorozirconic acid as simplified conversion solutions allows correlation of variations in chemisorption to the presence of zirconium oxide, whereas commercial solutions are characterized by increased surface complexity due to the presence of inorganic and organic additives (typically phosphates and acrylic polymers). Variations in surface chemistry due to zirconium-based conversion are evaluated by XPS and FE-AES surface analysis. Chemisorption studies are conducted using dimethylsuccinate molecules mimicking industrially relevant polyester resins. ATR-FTIR and XPS are used complementary to reveal bonding mechanisms on one hand and to semi-quantify the amount of interfacial bonds on the other hand. Therefore, to keep the oxide chemistry constant, characterization is consistently performed on thermally vaporized metal substrates.

2. Experimental

2.1. Materials and chemicals

50 nm zinc (Goodfellow, 99.95%), aluminium (Johnson Matthey, 99.99%) and magnesium (Alfa Aesar, 99.9%) were deposited on germanium internal reflection elements (IRE) by means of a high-vacuum evaporation system (VCM 600 Standard Vacuum Thermal Evaporator, Norm Electronics). Zirconium-based conversion was conducted using a home-made model conversion solution, prepared by diluting hexafluorozirconic acid (Sigma-Aldrich Chemistry) to 0.01 M using demineralized water and brought to pH 4 with 0.1 M NaOH. The use of a model conversion solution excludes interfacial effects of organic and inorganic additives. The metallic coated IREs were dipped in conversion solution at room temperature (22 ± 1 °C) for 90 s, where after the samples were generously rinsed with demineralized water and dried with pressurized air. Dimethylsuccinate (Sigma-Aldrich Chemistry) has been chosen to represent ester-functionalities specific to industrially relevant polyester resins commonly used in coil coats. This relatively small and thus mobile molecule has two highly accessible ester functionalities which is expected to enhance chemisorption. In line with previous work on the chemisorption succinic acid [38], dimethylsuccinate has been used in a concentration of 0.1 wt% dissolved in tetrahydrofuran (THF) whereafter the metal substrates were placed in solution for 30 min, dried in air and measured with ATR-FTIR before (combination of strongly and weakly interacting dimethylsuccinate) and after rinsing with pure THF (solely strongly interacting dimethylsuccinate) [38].

2.2. Attenuated total reflection – Fourier transform infrared spectroscopy (ATR-FTIR) in Kretschmann configuration

The FTIR apparatus was a Thermo-Nicolet Nexus equipped with a liquid-nitrogen cooled mercury-cadmium-telluride (MCT) detector and a nitrogen-purged measurement chamber with a Veemax III single reflection ATR accessory. Germanium internal reflection elements (PIKE Technologies) were used with a fixed face angle of 60°. IR-light was conFig.d with an incident set angle of 80°. For the chemisorption studies infrared backgrounds were obtained from the metallic coated IREs, after zirconium-based treatment when applicable. Infrared spectra were averaged from 128 cycles with a resolution of 4 cm^{-1}. The control of the spectra acquisition and incident angles was managed by the OMNIC 8.1 software package (ThermoElectron Corporation, Madison, WI).

2.3. X-ray photoelectron spectroscopy (XPS)

measurements were done with a PHI-5000 Versaprobe II (Physical Electronics) utilizing an Al Kα monochromatic X-ray source (1486.71 eV photon energy) with a spot diameter of 100 μm to measure surface compositions up to ca. 10 nm in depth. The irradiation power of

the X-ray beam was 25 W. The kinetic energy of the photoelectrons was measured with a take-off angle of 45°. The vacuum in the analysis chamber was better than 1×10^{-9} Torr. Survey scans were recorded with a pass energy of 187.85 eV and energy step size of 0.1 eV. The XPS data was analyzed with PHI Multipak software (V9.5). High resolution scans of O 1s, C 1s, F 1s, Zr 3d, Zn 2p3, Al 2p and Mg 1s were obtained with a pass energy of 23.5 eV and 0.05 eV energy step size. Dual beam charge neutralization was utilized to compensate potential charging effects. The high resolution O 1s and C 1s XPS peaks were fitted using Multipak (V9.8) software. Before curve fitting, the energy scale of the XPS spectra was calibrated relative to the binding energy of adventitious hydrocarbons (C C/C H) in the C 1s peak at 284.8 eV. The peak shape is a mixed Gaussian-Lorentzian, with a Shirley type background.

2.4. Field emission auger electron spectroscopy (FE-AES)

High-resolution mappings of the zirconium oxide coating were obtained using a JEOL JAMP9500F FE-AES spectrometer, employing an electron beam of 10 keV and 10.6 nA at an angle of incidence of 30°. The utilized magnification was x3000 for converted aluminium, x10,000 for converted magnesium and x20,000 for converted zinc. This resulted in mapping areas of approximately 35 × 35 µm for aluminium, 12 × 12 µm for magnesium and 6 × 6 µm for zinc. The data was extracted and processed using the JEOL Image Investigator V1.04 software.

3. Results

3.1. XPS metal oxide characterization

Thermally vaporized metallic layers were characterized using XPS analysis. Survey scans elucidated carbon, oxygen and metal signals on the native oxides. After zirconium-treatment, also zirconium and fluoride were traced on all converted oxide layers. An example of the survey scan for zirconium-treated zinc is presented in Fig. 1.

The elements identified in the survey scan are expressed in atomic percentages, using the relative sensitivity factors provided by the manufacturer. The resulting elemental surface composition is illustrated in Fig. 2. Fig. 2(a) compares the carbon (C), oxygen (O) and metal (M) contributions at the surface before (Native) and after (ZrCC) zirconium-treatment. This illustrates an increase in surface oxygen concentration after zirconium-treatment of zinc, aluminium and magnesium, while surface carbon and metal concentrations are being reduced. The reduction of surface carbon is attributed to the removal of ambient carbon contamination, resulting in a cleaner surface. The reduction of surface metal concentrations relates to the deposition of zirconium oxide. The atomic concentration of zirconium (Zr), metal (M) and fluor (F) after zirconium-treatment (ZrCC) is illustrated in Fig. 2(b). Significant variations in metal concentrations are being observed after zirconium-treatment of zinc (22 At. %), aluminium (14 At. %) and magnesium (8 At. %). Whereas more or less constant concentrations of zirconium oxide (ca 7 At. %) are being observed. Surface concentrations of fluorides are minor (1–2 At. %) in case of zinc and magnesium and reach approximately 5 At.% in case of converted aluminium. This is in line with reported stability constants for fluoride complexes, which are reported to increase in following order; Zn^{2+} (K = 0.8–1), Mg^{2+}(K = 1.3), Al^{3+} (K = 6–7) [39]. Reported stability constants for Zr^{4+} (K = 5) do not take into account the extent of zirconium hydrolysis in the presence of fluorides [39].

3.2. FE-AES elemental surface mappings

FE-AES mappings, shown in Fig. 3, were performed to evaluate the elemental distribution of the converted oxide layers. The white squares implemented in the FE-AES mappings define a 5 × 5 µm area demonstrating homogeneous lateral elemental distribution in the micrometer scale. Since molecular interfacial interactions take place on the nanometer scale, homogeneity of the converted oxide layers is thus shown to exist on a higher order of magnitude. Notable intensities of both aluminium and zirconium, given in Fig. 3 (a) and (b) respectively, indicate a mixed conversion oxide with aluminium and zirconium oxide coexisting at the outer surface. On the other hand, minor intensities of zinc and magnesium, shown in Fig. 3(c) and (e), together with the higher intensities observed for zirconium, given in Fig. 3(d) and (f), demonstrate that the outer surface of zirconium-treated zinc and magnesium oxide solely exists of zirconium oxide. As a result, molecular interactions on zirconium-treated zinc and magnesium substrates are taking place with zirconium oxide, whereas in case of zirconium-treated aluminium molecular interactions can take place on both aluminium and zirconium oxide.

Based on the obtained FE-AES mappings, a graphical representation of the converted oxides is given in Fig. 4. It should be noted that oxide thickness variations are not taken into account in Fig. 4. However, since the elemental surface composition obtained by XPS (given in Fig. 2) indicates the presence of zinc and magnesium, whereas these are shown to be absent at the outer zirconium oxide surface according to FE-AES mappings, the respective zirconium oxide layers are expected to be thicker than 3 nm, but thinner than 10 nm This because the sampling depth for XPS is known to be 3–10 nm for AlKα radiation [40].

3.3. Quantification surface hydroxide densities

The formation of a zirconium–based conversion layer is known to be a pH-based reaction in equilibrium with surface OH densities [41]. Because metal hydroxides are known to be important binding sites for

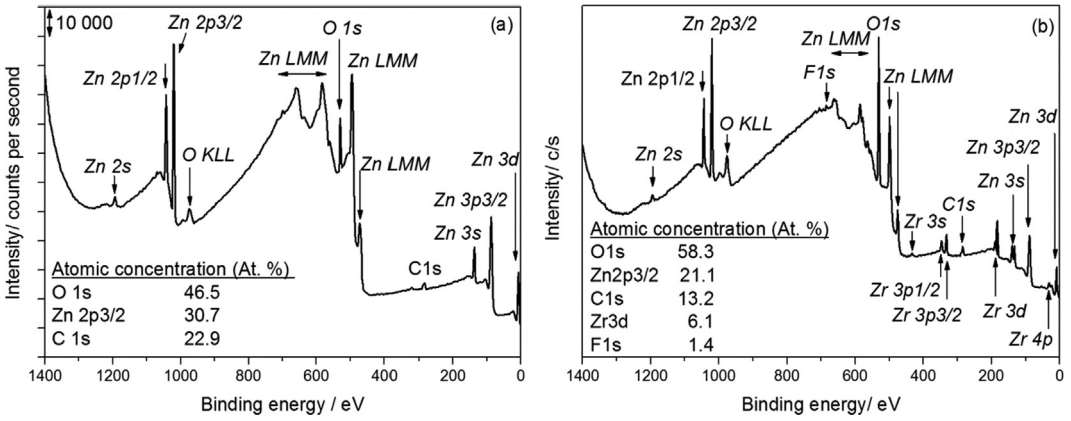

Fig. 1. Survey scan and the resulting elemental concentration of (a) native zinc oxide and (b) zirconium-treated zinc oxide.

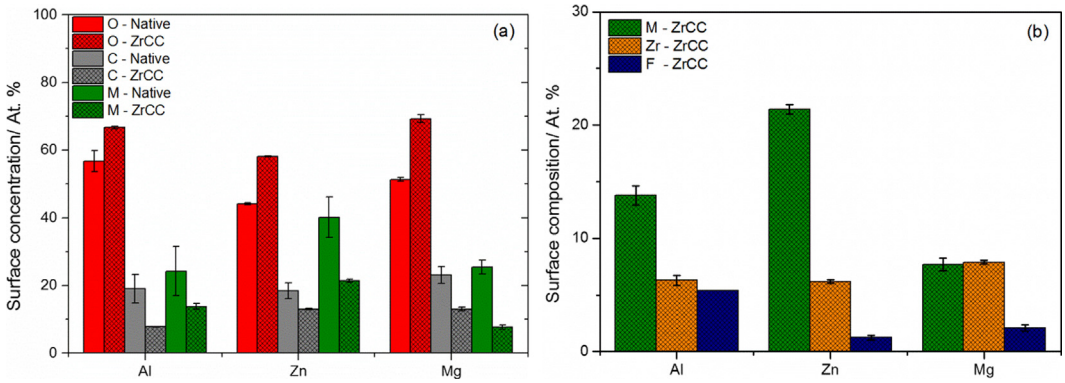

Fig. 2. Elemental surface composition (a) relative surface contributions oxygen, carbon and metal (Zn, Al, Mg) on native oxides (Native) and zirconium-treated (ZrCC) PVD substrates, (b) relative surface contributions of metal, zirconium and fluoride on hexafluorozirconic acid treated PVD substrates.

molecule interactions, their densities are being evaluated using O1s XPS analysis. Normalised high resolution XPS O 1s peaks before and after chemical conversion are shown in Fig. 5(a–c). The O^{2-} component specific to metal oxide, is positioned at 529.9 eV ± 0.3 eV [42]. Similar binding energies are expected in case of ZnO, Al_2O_3, MgO and ZrO_2. Therefore, no distinction can be made between metal and zirconium oxide based on the O 1s XPS peak. A second component, OH^- specific to metal hydroxide contributions is positioned at 531.5 ± 0.2 eV [42]. It is evidenced that the O^{2-} component reduces relative to OH^- component after zirconium-treatment indicating increased hydroxide densities at the metal surface after conversion. A third component assigned to chemisorbed water is positioned at 532.6 ± 0.3 eV [42]. By deconvoluting the O 1s XPS peak into its subcomponents, surface hydroxide fractions before and after zirconium-treatment can be estimated.

Surface hydroxide quantification is done using the approach proposed by McCafferty and Wightman [43]. This approach represents metal oxide as a multilayer system composed of discrete layers in depth, whereas lateral effects are averaged in the measured spot size of 100 μm. This model, illustrated in Fig. 6, assumes homogeneity of the discrete layers. The composition of this multilayer system consists of an overlayer of adsorbed organic contamination (t) covering the converted metal oxide layer. Underneath the contamination layer, an outermost oxide layer with a hydroxylated region of chemisorbed water exists. This outermost oxide layer consist of zirconium oxide in case of zirconium-treated substrates under which a pure innermost metal oxide layer is expected. Based on XPS and FE-AES data illustrated in Figs. 2 and 3, these two discrete layers are both being probed using XPS. Therefore, their properties (σ and λ) are being averaged as illustrated in Table 2.

The thickness (t), of the carbon contamination layer can be estimated by Eq. (1), described by Smith et al. [44]

$$t = -\lambda_{C1s} cos\Theta ln(1 - C1s/100) \quad (1)$$

With λ_{C1s} being 2.3 nm, which is the effective electron attenuation length for carbon 1 s photoelectrons in the carbon contamination layer, Θ the take-off angle relative to the surface normal. Values for C 1s, being the concentration of carbon expressed in atomic %, are given in Fig. 2(a). The estimated thickness (t) of carbon contamination on the respective oxides are presented in Table 1.

The measured O 1s signal contains contributions from the oxide matrix and was deconvoluted into three contributions (O^{2-}, OH and H_2O) as illustrated in Fig. 7 (a). Next to contributions of the oxide matrix also contributions from the carbon contamination layer (C-O, COO^-, O-C = O) are included in the O 1s peak. Because of the negligible differences in binding energy, OH contributions cannot be differentiated from those contributions specific to carbon contaminations. Therefore, a correction of the OH subpeak has to be made to avoid overestimation of surface hydroxyls due to the presence of organic contaminants. The XPS peak intensities (subpeak areas) of the respective contributions are obtained by C 1s and O 1s high resolution XPS curve fitting, as illustrated in Fig. 7(a) and (b) respectively. The fitting parameters used are given in supplementary information. From the assessed peak areas for oxygen bonded carbon (C-O, COO^- and O-C = O), a correction can be made for the overestimation of OH^- subpeak area, according to Eq. (3).

$$I^*_{OH} = \frac{I_{C-O} + I_{COO-} + I_{O-C=O}}{I_{OH}} \quad (3)$$

The corrected hydroxide sub peak intensity (I^*_{OH}) are correlated to the unknown concentrations of OH- (COH) and O2- (CO2-) according to Eqs. (4) and (5), which have been described extensively in earlier work [25,42,45].

$$C_{OH} = \frac{\sigma_C \lambda_C \left(1 - e^{-t/\lambda_C sin\Theta}\right) - I_1 \sigma_O \lambda_O \left(1 - e^{-t/\lambda_O sin\Theta}\right)}{I^*_{OH} \sigma_O \lambda_O \left(1 - e^{-t/\lambda_O sin\Theta}\right)} \quad (4)$$

$$C_{O2-} = \frac{\sigma_C \lambda_C \left(1 - e^{-t/\lambda_C sin\Theta}\right)}{I_{O2} - \sigma_O \lambda_O \left(1 - e^{-t/\lambda_O sin\Theta}\right)} \quad (5)$$

σ, the photoionization cross-section of the component of interest and λ, the inelastic mean free path of electrons specific to the component of interest. The latter describes the mean distance that an electron travels through a solid before losing energy. Consequently, the intensity attenuation of elements in the oxide layer by the covering ambient carbon contamination layer are taken into account when calculating the oxide elemental concentrations. The values for λ and σ are oxide specific and summarized in Tables 2. Solving these equations allow calculation of the surface hydroxide fraction using Eq. (6).

$$Hydroxyl\ \ fraction = \frac{1}{1 + \frac{C_{O2-}}{C_{OH}}} \quad (6)$$

Fig. 8 illustrates the estimated hydroxide fractions of native and zirconium-treated zinc, aluminium and magnesium oxide. It becomes clear that zirconium-treatment results in a substantial increase of surface hydroxide fraction varying between 80 and 90%. The high hydroxide coverages, nearly saturating the surface, likely relates to the active oxides of thermally vaporized films. Because of this, the fluoride concentration of the conversion solution is rather high resulting in aggressive dissolution of the native oxide [48]. High rates of accompanying oxygen reduction reactions cause local alkalinisation which is held responsible for the precipitation of zirconium oxide [41,49]. Yet, because of the high kinetics, accumulating hydroxides are expected to be incorporated in the precipitated zirconium oxide layer, as illustrated by the estimated hydroxide fractions in Fig. 8 [41,50].

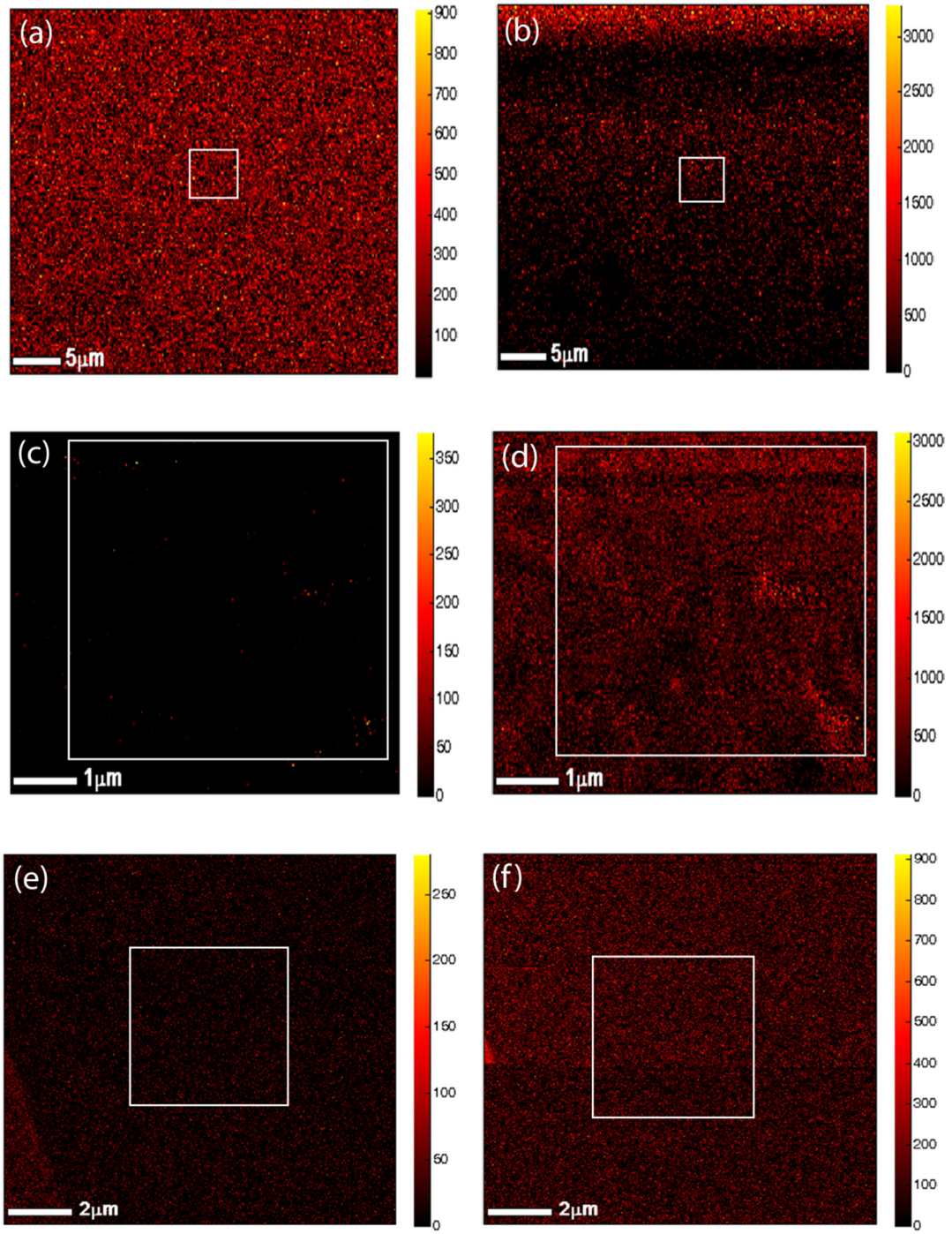

Fig. 3. FE-AES mappings obtained after zirconium-treatment, (a) aluminium and (b) zirconium distribution after conversion of aluminium, (c) zinc and (d) zirconium distribution after conversion of zinc, (e) magnesium and (f) zirconium distribution after conversion of magnesium.

3.4. ATR-FTIR study of ester-functionalized monomer chemisorption: dimethylsuccinate

ATR-FTIR studies of dimethylsuccinate molecules dissolved in THF (0.1 wt%) were performed on chemically inert germanium internal reflection elements (IRE). Fig. 9 illustrates the FTIR spectrum of bulk dimethylsuccinate obtained in the absence of a metallic oxide layer. The sharp peak at 1743 cm^{-1} is characteristic for the carbonyl (C = O) stretching vibration. The peaks at 1456 cm^{-1} and 1363 cm^{-1} are assigned to CH_2 and CH_3 bonds respectively [51]. The multiple bands in the 1200 cm^{-1} region correspond to C-O-C vibrations [51].

The three metals under investigation (Zn, Al and Mg) were deposited on germanium internal reflection elements by means of physical vapour deposition and immersed for 30 min in THF containing 0.1 wt% dimethylsuccinate molecules. After immersion the oxides were dried by solvent evaporation and analysed using ATR-FTIR. The resulting spectra, shown in Fig. 10(a), are associated to a combination of chemisorbed, physisorbed and possibly some non-interacting molecules. The subsequent rinsing step with pure THF solvent is supposed to remove those non- and weakly interacting dimethylsuccinate molecules. Therefore, the resulting spectra presented in Fig. 10(b) represent strongly interacted dimethylsuccinate.

Fig. 10(b) shows a reduced IR-frequency for carbonyl (C = O) peak in the presence of aluminium oxide (1731 cm^{-1}) compared to non-

Fig. 4. Graphical presentation oxide composition after zirconium-treatment.

interacted dimethylsuccinate (1743 cm^{-1}) as evidenced in Fig. 9. This shifts towards lower wavenumbers is associated to the involvement of carbonyl (C = O) oxygen atom in hydrogen bonds [26,28]. A similar shift can be seen for magnesium oxide. However, because of the low intensity of the carbonyl (C = O) peak which is in the order of the noise level, the establishment of interfacial hydrogen bonds are assumed to be negligible on magnesium oxide surface.

Furthermore, compared to the ATR-FTIR spectrum of bulk dimethylsuccinate (Fig. 9) an additional peak arises in the 1650–1500 cm^{-1} region in the presence of a metal film. The appearance of this additional peak is assigned to asymmetric carboxylate stretch vibrations and thus suggests the formation of carboxylate bonds upon interaction with the metal oxides under investigation [52]. The formed metal-carboxylate complexes are shown to be resistant to solvent rinsing, as illustrated by the remaining asymmetric carboxylate peak in Fig. 10(b).

Since carboxylate bonds originate from carboxylic acid species, the ester-groups of dimethylsuccinate are shown to hydrolyse in the presence of metal (hydr)oxide [33]. Hence, a two-step chemisorption mechanism is proposed, involving ester hydrolysis forming carboxylic acids followed by a deprotonation reaction giving carboxylate anion species, as illustrated in Fig. 11.

Varying asymmetric carboxylate (COO^{-}_{as}) peak positions depending on the interacting metal cation are being observed in Fig. 10(b). For aluminium, zinc and magnesium oxide, maximum asymmetric carboxylate peak intensities are noted at 1538, 1580 and 1585 cm^{-1}, respectively. Based on reported isoelectric points for aluminium, zinc and magnesium oxide (8, 9 and 12 respectively) [53], a correlation can be derived between the increasing IR-frequency of the asymmetric carboxylate stretch vibrations and the decreasing acidic nature of the metal cation. It has been reported that higher IR-frequencies for the asymmetric carboxylate stretching mode are associated to higher carboxylate bond strengths [54,55]. Hence, the carboxylate bond strength is shown to increase with increasing IEP (Al < Zn < Mg).

To summarize, two chemisorption mechanisms have been evidenced using ATR-FTIR in Kretschmann geometry. Both hydrogen-bonding and carboxylate bond formation were shown to depend on the metal-oxide acid-base properties. As such aluminium oxide demonstrated the highest tendency for hydrogen bonding. This is not surprising as its high positive charge (+III) is distributed on a relatively small ionic radius (Al 68 pm, Zn 88 pm, Mg 86 pm) [56,57] making aluminium cations most acidic. The high positive charge of aluminium cations strengthen the Al-OH bonds with hydroxide end-groups. This Al-OH bond strength is further enhanced by electron donation from the electron-rich carbonyl oxygen atom. Moreover, the electron donation by carbonyl oxygen atoms satisfies the electron affinity of acidic Al(III) cations resulting in strong interfacial hydrogen bonds between

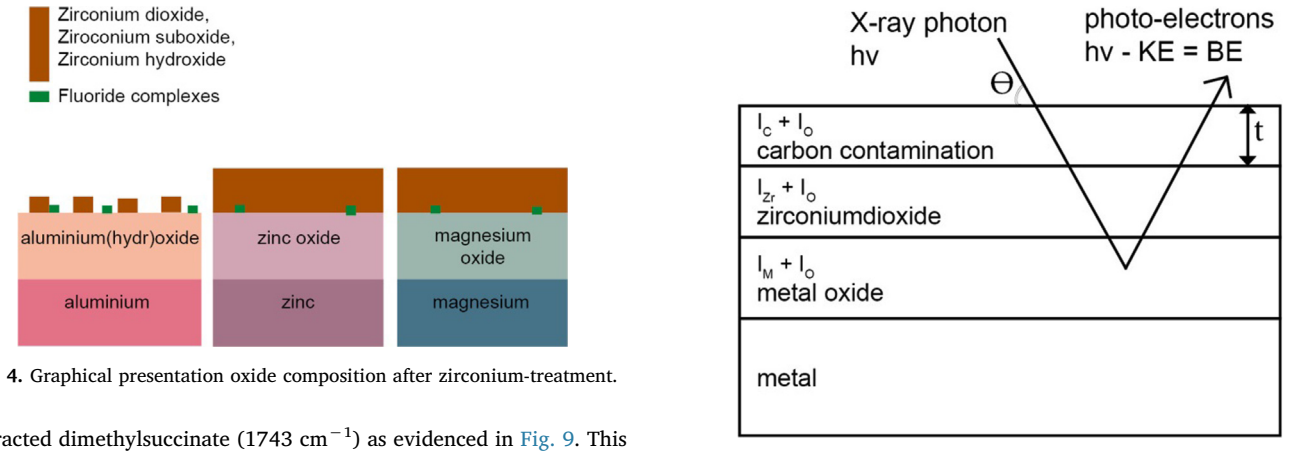

Fig. 6. Model used to describe the oxide composition of zirconium-treated zinc.

Table 1
Calculated thickness ambient carbon contamination.

t/nm	Native oxide	H_2ZrF_6 treated oxide
Zinc	0.5	0.3
Aluminium	0.5	0.2
Magnesium	0.6	0.3

Table 2
Photo-ionisation cross-sections (σ) and inelastic mean free paths (IMFP, λ) and used for quantifying surface hydroxide and oxide concentrations (Eqs. (5) and (6)).

Element	Photo-ionization cross-section (σ) [46]	Inelastic mean free path (λ)/ nm [47]
C	0.192	2.583
O (Al_2O_3)	0.523	2.251
O (ZnO)	0.523	1.870
O (MgO)	0.523	2.324
O (ZrO_2)	0.523	1.858
O (average)	0.523	2.076

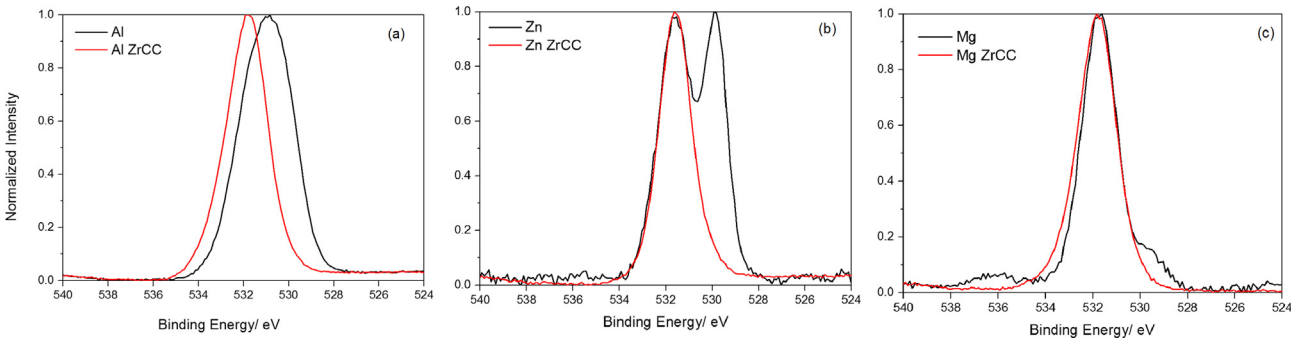

Fig. 5. High resolution O1s XPS peak before and after hexafluorozirconic acid treatment of (a) aluminium, (b) zinc and (c) magnesium.

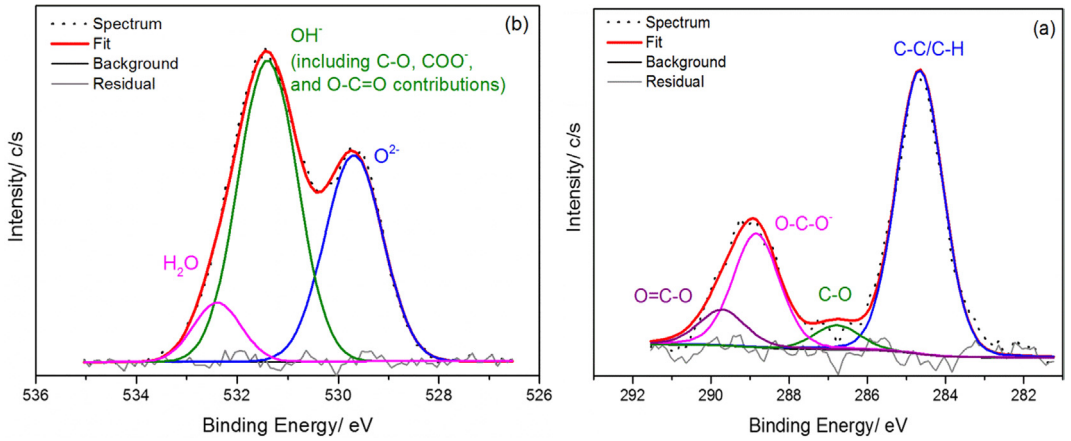

Fig. 7. Curvefit of (a) O 1s high resolution XPS peak and (b) C 1s high resolution XPS peak of a zinc substrate with native oxide.

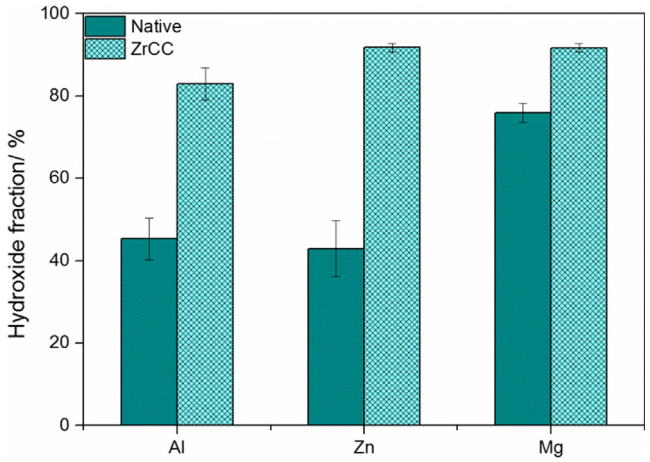

Fig. 8. Calculated hydroxide fractions before (native) and after (ZrCC) zirconium-treatment.

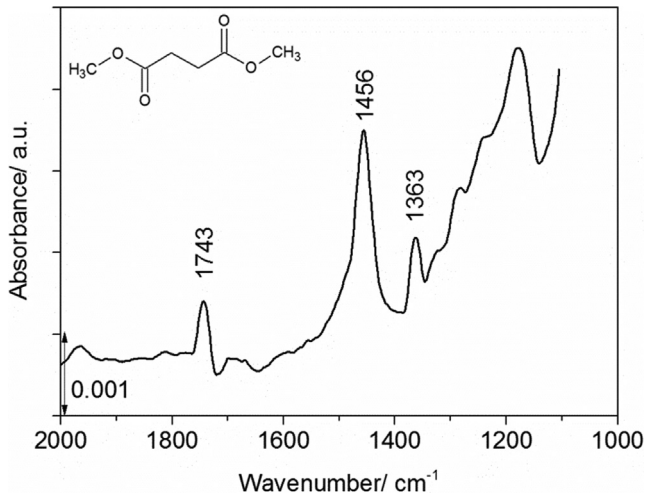

Fig. 9. ATR-FTIR spectrum of bulk dimethylsuccinate applied on germanium IRE by THF solvent evaporation.

aluminium hydroxide and dimethylsuccinate carbonyl groups, as illustrated in Fig. 12. On the other hand, more basic metal cations have less strong metal-hydroxide bonds. As a result they are characterized by a higher ability to donate these hydroxide end-groups, making them available for ester hydrolysis or carboxylic acid deprotonation as demonstrated in Figs. 11 and 12.

Subsequently, the effect of zirconium-treatment on the chemisorption mechanism of dimethylsuccinate molecules is investigated. The same procedure was repeated for the three metal substrates after a 90 s dip in H_2ZrF_6 0.01 M (pH 4). The resulting spectra before and after rinsing physisorbed molecules with THF are presented in Fig. 13 (a) and (b) respectively. Fig. 13 (a) points out that also after zirconium-treatment, interfacial carboxylate bonds are being formed on all three metal substrates. After washing off physisorbed molecules, carboxylate bonds remain present, demonstrating the stability of the chemical interfacial bonds. Remarkable is the absence of carbonyl bonds at the magnesium surface, suggesting that dimethylsuccinate is fully hydrolysed and coordinated to zirconium converted magnesium in a two-end adsorption mode. The IR-frequencies observed after rinsing, given in Figs. 10(b) and 13(b) are summarized in Table 3. It can be seen that the carbonyl (C = O) peak on both zinc and aluminium shifts towards lower wavenumbers, indicating its involvement in hydrogen bonds. A larger shift of the carbonyl peak is observed for both native aluminium oxide (12 cm^{-1}) and zirconium-treated aluminium oxide (11 cm^{-1}) compared to that for native zinc (2 cm^{-1}) and zirconium-treated zinc oxide (6 cm^{-1}). The increased shift after zirconium-treatment of zinc compared to native zinc oxide suggest that zirconium oxide increases the surface acidity, thereby increasing hydrogen donating properties.

Table 3 summarizes the observed carboxylate peak positions depending on the interacting cation. From these values, band separation between asymmetric and symmetric carboxylate stretch absorption bands can be determined which are typically indicative for the coordination mode. A minor shift of the separation values ($\Delta\nu_{as\text{-}s}$) for adsorbed dimethylsuccinate species compared to the succinate ion indicates the formation of a bridging bidentate surface complex [58,59]. Separation values significantly smaller than these observed for succinate ion suggest chelating bidentate (CB) coordination [58,59]. Separation values of 157 cm^{-1} are reported for succinate ions [58]. Hence, a bridging bidentate (BB) coordination is proposed to be formed on all metal oxides studied. Only native aluminium oxide gives a significantly lower separation value, which suggests the formation of chelating complexes. It is evidenced from the ATR-FTIR spectra in Figs. 10 and 13 that carboxylate peaks are subjected to band broadening, which is a general feature of adsorbed carboxylate species [58]. Therefore, it cannot be excluded that a combination of bridging and chelating bidentate coordination exist at the respective oxide surfaces. Furthermore, the IR-frequencies of carbonyl (C = O) bonds indicative for hydrogen bonding (HB) are summarized in Table 3. The lack of carbonyl (C = O) peak on magnesium substrates is associated to a two-end adsorption. The suggested coordination modes on aluminium, zinc and magnesium oxide are depicted in Fig. 14(a-c).

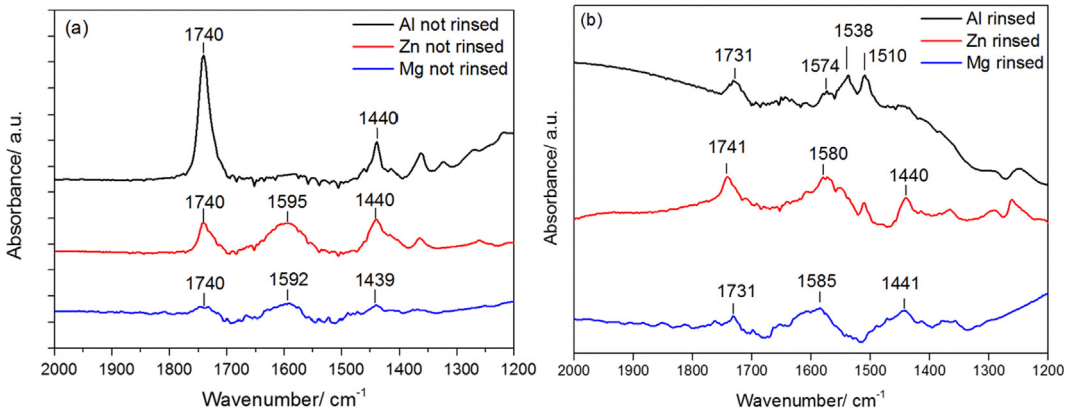

Fig. 10. Adsorption dimethylsuccinate molecules onto native metal oxides (a) combination of weakly and strongly interacting molecules before THF solvent rinsing (b) strongly interacting dimethylsuccinate molecules resistant to THF solvent rinsing.

3.5. XPS study of ester-functionalized monomer chemisorption: dimethylsuccinate

Based on the presented ATR-FTIR data, it becomes clear that the oxide acid-base properties determine the chemical interactions taking place with ester-functionalized molecules. XPS surface analysis demonstrated increased hydroxide fractions after zirconium- treatment which act as binding sites for both hydrogen interactions as well as ester-hydrolysis reactions. Nevertheless, no unambiguous statement can be made on the increased quantity of interfacial bonds due to zirconium-treatment based on the ATR-FTIR results. This because the IR-absorptive properties of the metal oxides as well as small variations in layer thickness hinder direct comparison of ATR-FTIR peak intensities between different oxides. Therefore, XPS studies have been performed to quantify the amount of established interfacial carboxylate bonds.

Fig. 15 presents the C 1s signal of native zinc oxide before and after dimethylsuccinate (DMS) adsorption. A chemical shift of oxygen bonded carbon towards lower binding energies suggests an increase in surface carboxylate species (COO^-) which has a characteristic binding energy at 288.5 eV [33,60]. All converted metal oxides exhibit such a chemical shift, suggesting increased portion of carboxylate species after dimethylsuccinate adsorption, which is in line with the observations obtained by ATR-FTIR.

The carbon signal resulting from the ambient contamination overlayer, could be deconvoluted into following subpeaks; C-C/C-H, C-O, COO^-, O-C = O, as illustrated in Fig. 7. A similar approach, validated by Pletincx et al. [33,60], has been implemented on native and zirconium-treated metal oxides after dimethyl succinate adsorption to quantify the amount of carboxylate species on the respective oxide surfaces. The quantified carboxylate (COO^-) subpeak areas before and after dimethylsuccinate chemisorption are normalized using the total C 1s peak area and summarized in Fig. 16. It is evidenced that zirconium-treatment does not increase the amount of adsorbed carboxylate species compared to native oxides. Subtracting quantified carboxylate species obtained before adsorption (bare) from those obtained after dimethylsuccinate adsorption (DMS) gives the net increase in carboxylate species indicated by the red arrows in Fig. 16.

This net increase of carboxylate species is shown to remain equal after zirconium-treatment of zinc and magnesium and reduces after zirconium-treated aluminium. However, it is expected that during adsorption ambient carbon contaminants are being replaced. Therefore, this net increase underestimates the amount of established interfacial carboxylate bonds. When comparing the total amount of carboxylate species after dimethylsuccinate adsorption a significant reduction is being observed after zirconium-treatment, indicated by the black arrows in Fig. 16. It was demonstrated that zirconium-treatment of thermally vaporized metal films results in highly hydroxylated surfaces. Although surface hydroxides are a requirement for carboxylate bond formation with dimethylsuccinate molecules due to the hydrolysis intermediate step, overhydroxylation might hinder accessibility of Lewis acid bonding sites for adsorption. Two reasons for such a poisoning effect have been described by Bjelopavlic et al. [61] Firstly, the Lewis acidity of the surface, related to the excess positive charge of metal cations, may become neutralized by the presence of negatively charged hydroxyl groups. Secondly, the cations (Lewid acid sites) are physically buried due to neighbouring hydroxide groups (Bronsted acid sites), as illustrated in Fig. 17. In that case, Lewis acid sites exist in holes, which might not be sterically accessible for bridging bidentate carboxylate bond formation. Under these circumstances, it can be expected that the establishment of interfacial bonds on Bronsted acid sites, being the formation of hydrogen bonds between dimethylsuccinate oxygen atom and zirconium hydroxide proton, becomes more favourable, as illustrated in Fig. 17. This was also indicated by ATR-FTIR, since the ester carbonyl peak shift towards lower wavenumbers after zirconium-treatment of zinc, indicating increased affinity for hydrogen bonding after zirconium-treatment. Hence, tuning the surface hydroxides

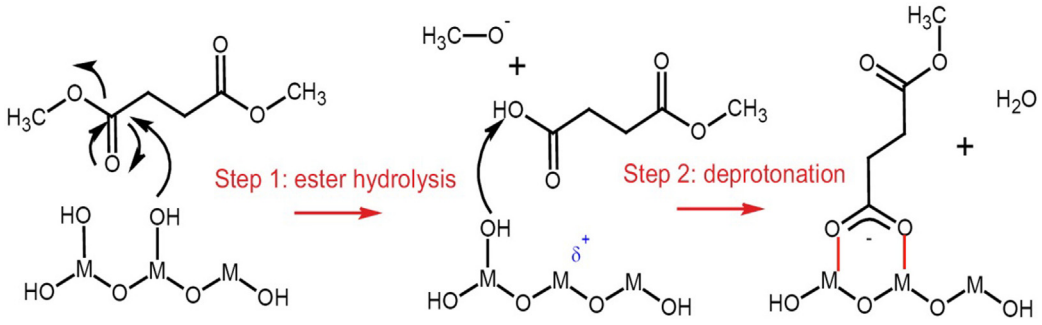

Fig. 11. Proposed chemisorption mechanism for dimethylsuccinate resulting in interfacial metal carboxylate bond formation.

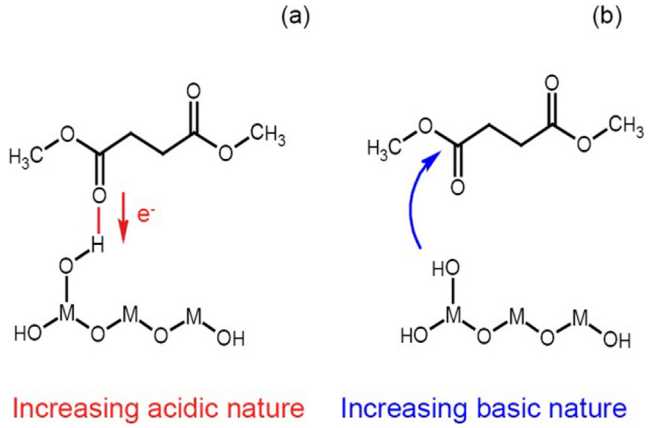

Fig. 12. The determining role of metal oxide acid-base properties in the preferred chemisorption mechanism: (a) increased acidic nature enhancing hydrogen bonding, (b) increased basic nature enhancing carboxylate bond formation.

density, to meet requirements for carboxylate anion formation by ester hydrolysis and deprotonation without poisoning Lewis acid sites is suggested to be crucial for maximum interfacial carboxylate bond formation.

ATR-FTIR in Kretschmann configuration has shown to provide valuable information regarding the role of oxide acid-base properties on the revealed chemisorption mechanisms. Nevertheless, this technique requires the use of model metal substrates (thermally vaporized nanolayers) which raises the question of the relevance of the obtained information for realistic metal-polyester hybrid systems. Whereas this current work focussed on the complementarity of ATR-FTIR and XPS using model substrates consistently, it is suggested to continue interfacial XPS studies using realistic bulk substrates to further investigate the correlation between surface hydroxide fractions and carboxylate bonding. Furthermore, additional attention is required for the susceptibility of the established interfacial bonds to the introduction of aqueous media. In line with this, the corrosion resistance of zirconium-treated substrates is another highly relevant aspect of zirconium-based conversion coatings. To further investigate the correlation between adhesion and corrosion resistance, consecutive research has been conducted using in-situ ATR-FTIR on the effect of zirconium-treatment of multi-metal oxides on the chemisorption of industrially relevant polyester paints and their stability in aqueous environment [62].

4. Conclusions

Three main observations have been made regarding the effect of zirconium-treatment of thermally vaporized multi-metal oxides on their interactions with ester-functionalized molecules. Firstly, XPS analysis demonstrated a significantly increased surface hydroxide density upon zirconium-treatment. Quantification of the surface hydroxide fractions resulted in surface concentrations of 80–90% hydroxides. Secondly, ATR-FTIR analysis revealed the co-existence of two competing chemisorption mechanisms, i.e. hydrogen bonding and carboxylate bond formation and the determining role of metal oxide acid-base properties with respect to these competing chemisorption mechanisms. Thirdly, the amount of established interfacial carboxylate bonds was estimated by XPS C1s peak deconvolution. This lead to the conclusion that the amount of interfacial carboxylate bonds did not increase upon zirconium-treatment, which was associated to the increased hydroxide fraction.

Table 3
IR-frequencies of observed carbonyl and carboxylate stretching vibrations after rinsing weakly interacted dimethylsuccinate molecules using THF solvent rinsing and the respective coordination modes; Hydrogen bond (HB), Chelating bidentate (CB), Bridging bidentate (BB).

	$\nu C = O$ (cm^{-1})	$\nu COO^-_{(as)}$ (cm^{-1})	$\nu COO^-_{(s)}$ (cm^{-1})	$\Delta\nu_{as\text{-}s}$ (cm^{-1})	Coordination
Blanc	1743	–	–	157*	–
Al	1731	1538	1440	98	HB + CB
Zn	1741	1580	1440	140	BB
Mg	(1731)	1585	1441	144	BB
Al Zr	1732	1574	1436	138	HB + BB
Zn Zr	1737	1576	1438	138	HB + BB
Mg Zr	–	1585	1462	123	BB

* Succinate ion reference value [58].

Declaration of Competing Interest

The authors declare that they have no known competing financial interests or personal relationships that could have appeared to influence the work reported in this paper.

Acknowledgement

This research was carried out under project number F81.3.13509 in the framework of the Partnership Program of the Materials innovation institute M2i (www.m2i.nl) and the Foundation for Fundamental Research on Matter (FOM), which is part of the Netherlands Organisation for Scientific Research NWO (www.nwo.nl). S.P. would like to acknowledge financial support by Research Foundation-Flanders (FWO) under project number SB-19-151. The authors would also like to acknowledge Priya Laha for her assistance with the FE-AES

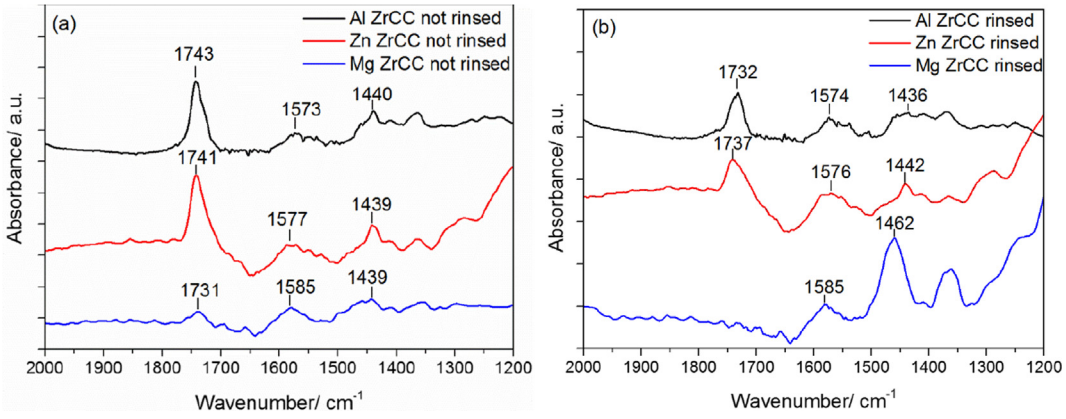

Fig. 13. Adsorption dimethylsuccinate molecules onto zirconium-treated metal oxides (a) combination of weakly and strongly interacting molecules before THF solvent rinsing (b) strongly interacting dimethylsuccinate molecules resistant to THF solvent rinsing.

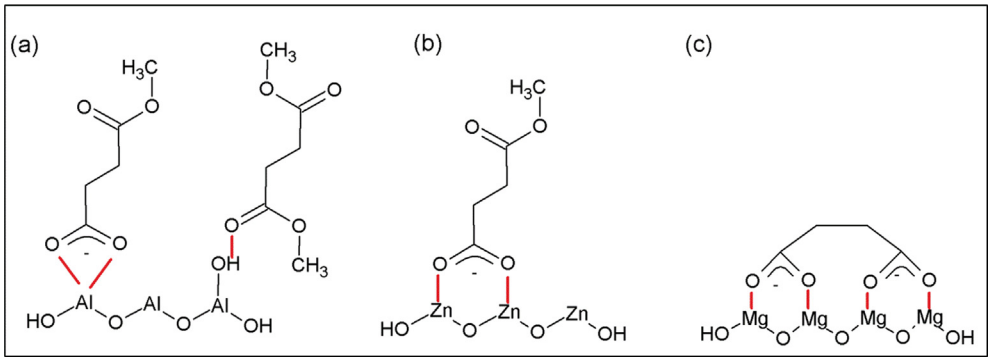

Fig. 14. Coordination modes of chemisorbed dimethylsuccinate on (a) aluminium, (b) zinc and (c) magnesium oxide interpreted from ATR-FTIR data.

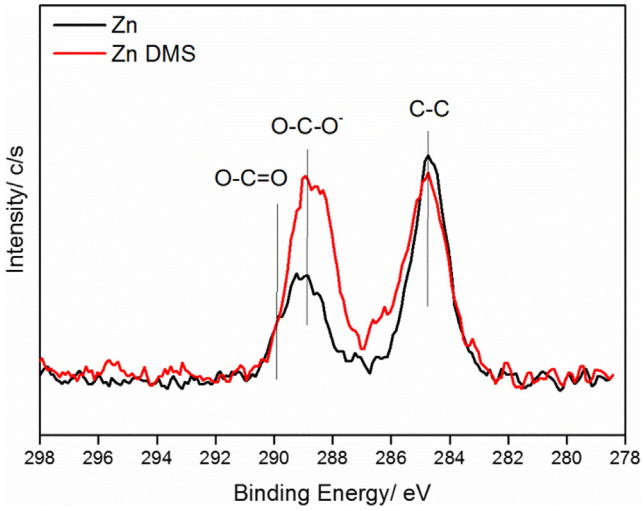

Fig. 15. High resolution C 1s carbon peak before and after dimethylsuccinate adsorption on native zinc oxide.

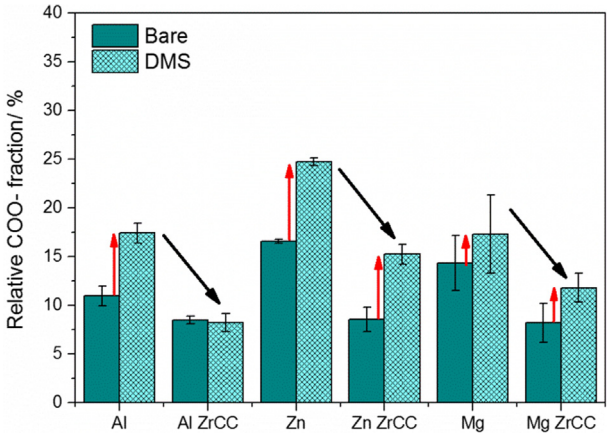

Fig. 16. Relative COO^- fractions (%) at metal oxide surface before (bare) and after (DMS) dimethylsuccinate adsorption.

measurements.

Authors contribution

L.I.F. wrote the main manuscript text. S.P., B.B., T.H., H.T. and J.M.C.M. all reviewed the manuscript text. All authors have given approval to the final version of the manuscript.

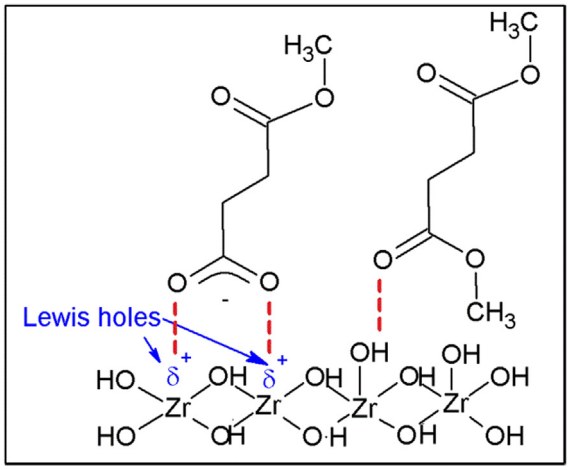

Fig. 17. Structural presentation of Lewis acid sites, sterically poisoned by surrounding Bronsted acid bonding sites on highly hydroxylated zirconium oxide.

Appendix A. Supplementary material

Supplementary data to this article can be found online at https://doi.org/10.1016/j.apsusc.2019.145199.

References

[1] J. Sullivan, S. Mehraban, J. Elvins, In situ monitoring of the microstructural corrosion mechanisms of zinc-magnesium-aluminium alloys using time lapse microscopy, Corros. Sci. 53 (6) (2011) 2208–2215.
[2] T. Prosek, A. Nazarov, U. Bexell, D. Thierry, J. Serak, Corrosion mechanism of model zinc-magnesium alloys in atmospheric conditions, Corros. Sci. 50 (8) (2008) 2216–2231.
[3] J. Elvins, J.A. Spittle, J.H. Sullivan, D.A. Worsley, The effect of magnesium additions on the microstructure and cut edge corrosion resistance of zinc aluminium alloy galvanised steel, Corros. Sci. 50 (6) (2008) 1650–1658.
[4] N.C. Hosking, M.A. Ström, P.H. Shipway, C.D. Rudd, Corrosion resistance of zinc-magnesium coated steel, Corros. Sci. 49 (9) (2007) 3669–3695.
[5] E. Zoestbergen, J.Van De Langkruis, T.F.J. Maalman, E. Batyrev, Surf. Coat. Technol. 309 (2017) 904–910.
[6] G. Yoganandan, K. Pradeep Premkumar, J.N. Balaraju, Evaluation of corrosion resistance and self-healing behavior of zirconium-cerium conversion coating developed on AA2024 alloy, Surf. Coatings Technol. 270 (2015) 249–258.
[7] N.W. Khun, G.S. Frankel, Composition and corrosion protection of hexafluorozirconic acid treatment on steel, Mater. Corros. 66 (11) (2015) 1215–1222.
[8] H. Ardelean, I. Frateur, P. Marcus, Corrosion protection of magnesium alloys by cerium, zirconium and niobium-based conversion coatings, Corros. Sci. 50 (7) (2008) 1907–1918.
[9] A. Ghanbari, M.M. Attar, Influence of phosphate ion on the morphology, adhesion strength, and corrosion performance of zirconium-based surface treatment, J. Coatings Technol. Res. (2015).
[10] R.R. Pareja, R.L. Ibáñez, F. Martín, D. Leinen, Corrosion behaviour of zirconia barrier coatings on galvanized steel, Surf. Coat. Technol. 200 (2006) 6606–6610.
[11] L. Fedrizzi, F. Rodriguez, S. Rossi, F. Deflorian, R. Di Maggio, The use of electrochemical techniques to study the corrosion behaviour of organic coatings on steel pretreated with sol-gel zirconia films, Electrochim. Acta 46 (2001) 3715–3724.
[12] X. Zuo, W. Li, S. Mu, J. Du, Y. Yang, P. Tang, Investigation of composition and

structure for a novel Ti–Zr chemical conversion coating on 6063 aluminum alloy, Prog. Org. Coatings 87 (2015) 61–68.
[13] S. Sharifi Golru, M.M. Attar, B. Ramezanzadeh, Effects of surface treatment of aluminium alloy 1050 on the adhesion and anticorrosion properties of the epoxy coating, Appl. Surf. Sci. 345 (2015).
[14] H.R. Asemani, P. Ahmadi, A.A. Sarabi, H. Eivaz Mohammadloo, Effect of zirconium conversion coating: adhesion and anti-corrosion properties of epoxy organic coating containing zinc aluminum polyphosphate (ZAPP) pigment on carbon mild steel, Prog. Org. Coatings 94 (2016) 18–27.
[15] A. Ghanbari, M.M. Attar, Surface free energy characterization and adhesion performance of mild steel treated based on zirconium conversion coating: a comparative study, Surf. Coatings Technol. 246 (2014) 26–33.
[16] P. Taheri, K. Lill, J.H.W. De Wit, J.M.C. Mol, H. Terryn, Effects of zinc surface acid-based properties on formation mechanisms and interfacial bonding properties of zirconium-based conversion layers, J. Phys. Chem. C 116 (15) (2012) 8426–8436.
[17] S. Verdier, S. Delalande, N. Van Der Laak, J. Metson, F. Dalard, Monochromatized X-ray photoelectron spectroscopy of the AM60 magnesium alloy surface after treatments in fluoride-based Ti and Zr solutions, Surf. Interface Anal. 37 (5) (2005) 509–516.
[18] F. Andreatta, a. Turco, I. de Graeve, H. Terryn, J.H.W. de Wit, L. Fedrizzi, SKPFM and SEM study of the deposition mechanism of Zr/Ti based pre-treatment on AA6016 aluminum alloy, Surf. Coatings Technol. 201 (18) (2007) 7668–7685.
[19] Y. Liu, Y. Yang, C. Zhang, T. Zhang, B. Yu, G. Meng, Y. Shao, F. Wang, L. Liu, Protection of AA5083 by a zirconium-based conversion coating, J. Electrochem. Soc. 163 (9) (2016) 576–586.
[20] N.W. Khun, G.S. Frankel, Effect of hexafluorozirconic acid pretreatment on cathodic delamination of epoxy coatings from steel substrates, Corrosion 71 (3) (2015) 277–284.
[21] P. Puomi, H.M. Fagerholm, J.B. Rosenholm, R. Sipila, Optimization of commercial zirconic acid based pretreatment on Hot-Dip galvanized and Galfan coated steel, Surf. Coatings Technol. 115 (1999) 79–86.
[22] S. Pletincx, L.L.I. Fockaert, J.M.C. Mol, T. Hauffman, T. Herman, Probing the formation and degradation of chemical interactions from model molecule/metal oxide to buried polymer/metal oxide interfaces, NPJ Mater. Degrad. 3 (23) (2019) 1–12.
[23] C. Boiziau, G. Lecayon, Adhesion of polymers to metals: a review of the results obtained studying a model system, Surf. Interface Anal. 12 (1988) 475–485.
[24] J. Marsh, L. Minel, M.G. Barthes-Labrousse, D. Gorse, Interaction of epoxy model molecules with aluminium, anodised titanium and copper surfaces: an XPS study, Appl. Surf. Sci. 133 (4) (1998) 270–286.
[25] J. Wielant, T. Hauffman, O. Blajiev, R. Hausbrand, H. Terryn, Influence of the iron oxide acid-base properties on the chemisorption of model epoxy compounds studied by XPS, J. Phys. Chem. C 111 (35) (2007) 13177–13184.
[26] J.Van Den Brand, O. Blajiev, P.C.J. Beentjes, H. Terryn, J.H.W.De Wit, Interaction of ester functional groups with aluminum oxide surfaces studied using infrared reflection absorption spectroscopy, Langmuir 20 (2004) 6318–6326.
[27] F.M. De Wit, Ö. Özkanat, J.M.C. Mol, H. Terryn, J.H.W. De Wit, The influence of pre-treatments of aluminium alloys on bonding of PET coatings, Surf. Interface Anal. 42 (4) (2010) 316–320.
[28] P.C.J. Beentjes, J. Van den Brand, J.H.W. De Wit, Interaction of ester and acid groups containing organic compounds with iron oxide surfaces, J. Adhes. Sci. Technol. 20 (1) (2006) 1–18.
[29] S.R. Leadley, J.F. Watts, The use of monochromated XPS to evaluate acid- base interactions at the PMMA/oxidised metal interface, J. Adhes. 60 (1997) 175–196.
[30] K. Konstadinidis, B. Thakkar, A. Chakraborty, L.W. Potts, R. Tannenbaum, M. Tirrell, J.F. Evans, Segment level chemistry and chain conformation in the reactive adsorption of poly(methylmethacrylate) on aluminum oxide surfaces, Langmuir 8 (5) (1992) 1307–1317.
[31] E. Papirer, J.M. Perrin, G. Nanse, P. Fioux, Adsorption of poly (methylmethacrylate) on an [alpha] alumina: evidence of formation of surface carboxylate bonds, Eur. Polym. J. 30 (8) (1994) 985–991.
[32] R. Tannenbaum, S. King, J. Lecy, M. Tirrell, L. Potts, Infrared study of the kinetics and mechanism of adsorption of acrylic polymers on alumina surfaces, Langmuir 20 (11) (2004) 4507–4514.
[33] S. Pletincx, K. Marcoen, L. Trotochaud, L.-L. Fockaert, J.M.C. Mol, A.R. Head, O. Karslioğlu, H. Bluhm, H. Terryn, T. Hauffman, Unravelling the chemical influence of water on the PMMA/aluminum oxide hybrid interface in situ, Sci. Rep. 7 (1) (2017) 13341.
[34] P. Taheri, J. Wielant, T. Hauffman, J.R. Flores, F. Hannour, J.H.W.De Wit, J.M.C. Mol, H. Terryn, A comparison of the interfacial bonding properties of carboxylic acid functional groups on zinc and iron substrates, Electrochim. Acta 56 (4) (2011) 1904–1911.
[35] F.M. De Wit, J.M.C. Mol, H. Terryn, J.H.W. De Wit, The influence of chemical pre-treatment and magnesium surface enrichment on bonding of succinic acid molecules to aluminium alloy the influence of chemical pre-treatment and magnesium surface enrichment on bonding of succinic acid molecules, J. Adhes. Sci. Technol. 22 (2008) 1089–1104.
[36] J. Cerezo, I. Vandendael, R. Posner, K. Lill, J.H.W. de Wit, J.M.C. Mol, H. Terryn, Initiation and growth of modified Zr-based conversion coatings on multi-metal surfaces, Surf. Coatings Technol. 236 (2013) 284–289.
[37] L.I. Fockaert, P. Taheri, S.T. Abrahami, B. Boelen, H. Terryn, J.M.C. Mol, Zirconium-based conversion film formation on zinc, aluminium and magnesium oxides and their interactions with functionalized molecules, Appl. Surf. Sci. 423 (2017) 817–828.
[38] P. Taheri, T. Hauffman, J.M.C. Mol, J.R. Flores, F. Hannour, J.H.W. De Wit, H. Terryn, Molecular interactions of electroadsorbed carboxylic acid and succinic anhydride monomers on zinc surfaces, J. Phys. Chem. C 115 (34) (2011) 17054–17067.
[39] A.M. Bond, G.T. Hefter, Critical Survey of Stability Constants and Related Thermodynamic Data of Fluoride Complexes in Aqueous Solution, Pergamon Press, Oxford, New York, 1980.
[40] C.J. Powell, A. Jablonski, I.S. Tilinin, S. Tanuma, D.R. Penn, Surface sensitivity of X-ray photoelectron spectroscopy, J. Electron Spectros. Relat. Phenomena 98–99 (1999) 1–15.
[41] P. Taheri, P. Laha, H. Terryn, J.M.C. Mol, An in situ study of zirconium-based conversion treatment on zinc surfaces, Appl. Surf. Sci. 356 (2015) 837–843.
[42] S.T. Abrahami, T. Hauffman, J.M.M. De Kok, J.M.C. Mol, H. Terryn, XPS analysis of the surface chemistry and interfacial bonding of barrier-type Cr(VI)-free anodic oxides, J. Phys. Chem. C 119 (34) (2015) 19967–19975.
[43] E. McCafferty, J.P. Wightman, Determination of the concentration of surface hydroxyl groups on metal oxide films by a quantitative XPS method, Surf. Interface Anal. 26 (8) (1998) 549–564.
[44] G.C. Smith, Evaluation of a simple correction for the hydrocarbon contamination layer in quantitative surface analysis by XPS, J. Electron Spectros. Relat. Phenomena 148 (2005) 21–28.
[45] T. Hauffman, O. Blajiev, J. Snauwaert, C. van Haesendonck, A. Hubin, H. Terryn, Study of the self-assembling of n -octylphosphonic acid layers on aluminum oxide, Langmuir 24 (5) (2008) 13450–13456.
[46] V. Nefedov, X-Ray Photoelectron Spectroscopy of Solid Surfaces, Taylor & Francis, 1988.
[47] S. Tanuma, C.J. Powell, D.R. Penn, Proposed formula for electron inelastic mean free paths based on calculations for 31 materials, Surf. Sci. Lett. 192 (1987) 849–857.
[48] S. Verdier, N. van der Laak, F. Dalard, J. Metson, S. Delalande, An electrochemical and SEM study of the mechanism of formation, morphology, and composition of titanium or zirconium fluoride-based coatings, Surf. Coatings Technol. 200 (9) (2006) 2955–2964.
[49] O. Lunder, C. Simensen, Y. Yu, K. Nisancioglu, formation and characterisation of Ti-Zr based conversion layers on AA6060 aluminium, Surf. Coatings Technol. 184 (2–3) (2004) 278–290.
[50] J. Cerezo, P. Taheri, I. Vandendael, R. Posner, K. Lill, J.H.W. de Wit, J.M.C. Mol, H. Terryn, Influence of surface hydroxyls on the formation of Zr-based conversion coatings on AA6014 aluminum alloy, Surf. Coatings Technol. 254 (2014) 277–283.
[51] George Socrates, Infrared and Raman Characteristic Group Frequencies, third ed., John Wiley & Sons Inc, 2001.
[52] H. Hu, J. Saniger, J. Garcia-Alejandre, V.M. Castaño, Fourier transform infrared spectroscopy studies of the reaction between polyacrylic acid and metal oxides, Mater. Lett. 12 (4) (1991) 281–285.
[53] M. Kosmulski, Isoelectric points and points of zero charge of metal (Hydr)Oxides: 50 years after parks' review, Adv. Colloid Interface Sci. 238 (2016) 1–61.
[54] P. Taheri, T. Hauffman, J.M.C. Mol, J.R. Flores, F. Hannour, J.H.W.De Wit, H. Terryn, Electrochemical analysis of the adsorption and desorption behaviors of carboxylic acid and anhydride monomers onto zinc surfaces, Electrochim. Acta 56 (25) (2011) 9317–9323.
[55] Y.T. Tao, Structural comparison of self-assembled monolayers of n-alkanoic acids on the surfaces of silver, copper, and aluminum, J. Am. Chem. Soc. 115 (10) (1993) 4350–4358.
[56] I.D. Brown, R.D. Shannon, Empirical bond-strength–bond-length curves for oxides, Acta Crystallogr. Sect. A 29 (3) (1973) 266–282.
[57] B.Y.R.D. Shannon, M. H, N.H. Baur, O.H. Gibbs, M. Eu, V. Cu, Revised Effective Ionic Radii and Systematic Studies of Interatomie Distances in Halides and Chaleogenides. Acta Crystallogr. Sect. A 32 (1976) 751–767.
[58] K.D. Dobson, A.J. Mcquillan, In situ infrared spectroscopic analysis of the adsorption of aliphatic carboxylic acids to TiO2, ZrO2, Al2O3, and Ta2O5 from aqueous solutions, Spectrochim. Acta - Part A Mol. Biomol. Spectrosc. 55 (1999) 1395–1405.
[59] V. Zelenak, Z. Vargova, K. Györyova, Correlation of infrared spectra of zinc(II) carboxylates with their structures, Spectrochim. Acta - Part A Mol. Biomol. Spectrosc. 66 (2) (2007) 262–272.
[60] S. Pletincx, L. Trotochaud, L.-L. Fockaert, J.M.C. Mol, A.R. Head, O. Karslıoğlu, H. Bluhm, H. Terryn, T. Hauffman, In Situ characterization of the initial effect of water on molecular interactions at the interface of organic/inorganic hybrid systems, Sci. Rep. 7 (2017) 45123.
[61] M. Bjelopavlic, E. Hassan, B.M. Moudgill, Polymers in particulate systems, Chapter 4, in: V.A. Hackley, P. Somasundaran, J.A. Lewis (Eds.), Role of Polymer Functionality in Specific Adsorption to Oxides: A Molecular Recognition Approach, New York, Dekker, 2002.
[62] L.I. Fockaert, S. Pletincx, D. Ganzinga-Jurg, B. Boelen, T. Hauffman, H. Terryn, J.M.C. Mol, Chemisorption of polyester coatings on zirconium-based conversion coated multi-metal substrates and their stability in aqueous environment, Appl. Surf. Sci. (2019), https://doi.org/10.1016/j.apsusc.2019.144771 (in press).